RBRH

Revista Brasileira de Recursos Hídricos
Brazilian Journal of Water Resources
Versão On-line ISSN 2318-0331
RBRH, Porto Alegre, v. 29, e2, 2024
Scientific/Technical Article

https://doi.org/10.1590/2318-0331.292420230089

Submerged hydraulic jump: a computational analysis in different scales

Ressalto hidráulico submergido: uma análise em diferentes escalas

João Pedro Paludo Bocchi[1], Daniela Guzzon Sanagiotto[1] & Eder Daniel Teixeira[1]

[1]Instituto de Pesquisas Hidráulicas, Universidade Federal do Rio Grande do Sul, Porto Alegre, RS, Brasil
E-mails: jp.bocchi@gmail.com (JPPB), dsanagiotto@ufrgs.br (DGS), eder.teixeira@ufrgs.br (EDT)

Received: August 24, 2023 - Revised: October 26, 2023 - Accepted: December 06, 2023

ABSTRACT

Advancements in computational capabilities have enabled engineers and scientists to numerically model complex turbulent phenomena such as hydraulic jumps. This research assesses the capability of numerically simulating a hydraulic jump that occurs in the UHE Porto Colômbia's stilling basin at a flow rate of 4,000 m^3/s. To achieve this, simulation results were compared with data from three hydraulic physical models (scales 1:32, 1:50, and 1:100) and full-scale measurements. The simulations employed the Ansys CFX solver, utilizing a Reynolds-Averaged Navier-Stokes (RANS) approach, the RNG κ-ε turbulence model, and the Volume of Fluid (VOF) method for air-water interactions. Various variables were analyzed, with satisfactory results for mean pressures, conjugated depths, roller length, water profile in less aerated areas, and mean velocity at the submerged hydraulic jump upstream section, with errors below 10%. However, the submerged hydraulic jump's start position and the representation of the water surface profile in the region near the jump toe yielded more disparate results. In conclusion, the methods and conditions applied in the simulations are apt for representing variables less impacted by aeration phenomena, establishing CFD simulations as a valuable tool for hydraulic jump analysis.

Keywords: Hydraulic jump; Submerged hydraulic jump; CFD; RANS.

RESUMO

A evolução da capacidade de processamento e memória dos computadores propiciou aos engenheiros e cientistas a modelagem numérica de fenômenos de natureza turbulenta complexa, tal como os ressaltos hidráulicos. Essa pesquisa avalia a capacidade de simular numericamente um ressalto hidráulico que ocorre na bacia de dissipação da UHE Porto Colômbia com uma vazão de 4,000 m^3/s. Para isso, os resultados das simulações foram comparados com dados medidos três modelos físicos hidráulicos (escalas 1:32, 1:50 e 1:100) e medições em protótipo. As simulações utilizaram o solver Ansys CFX, empregando uma abordagem baseada em nas equações médias de Navier-Stokes por decomposição de Reynolds (RANS), o modelo de turbulência RNG κ-ε e o método Volume of Fluid (VOF) para interações água-ar. Diversas variáveis foram analisadas, com resultados satisfatórios para pressões médias, profundidades conjugadas, comprimento do rolo, perfil da linha d'água em áreas menos aeradas e velocidade média na seção de montante do ressalto hidráulico submerso, com erros inferiores a 10%. No entanto, a posição de início do ressalto hidráulico submerso e a representação do perfil da superfície da água na região próxima ao pé do ressalto apresentaram resultados mais discrepantes. Em conclusão, os métodos e condições aplicados nas simulações são adequados para representar variáveis menos afetadas pelo fenômeno de aeração, estabelecendo as simulações em CFD como uma ferramenta valiosa para a análise de ressaltos hidráulicos.

Palavras-chave: Ressalto hidráulico; Ressalto hidráulico submergido; CFD; RANS.

INTRODUCTION

The hydraulic jump is a physical phenomenon characterized by the abrupt transition from an upstream supercritical flow upstream to a downstream subcritical flow. This phenomenon has intrigued scientists for at least two centuries, with notable studies such as Bidone's classic research in the early 19th century (De Padova & Mossa, 2021) and the development of the Bélanger Equation during the same period (Chanson, 2009a; De Padova & Mossa, 2021). Studies related to hydraulic jumps have gained significance due to their wide applicability in hydraulic engineering, owing to their turbulent characteristics that result in high energy dissipation during their occurrence. As a result, the presence of this phenomenon becomes attractive in energy dissipation structures within dam safety systems, such as hydraulic jump stilling basins (Prá, 2011).

In addition to the analytical description of this phenomenon, the use of hydraulic physical models, through their instrumentation and analysis of collected data, is one of the oldest methods for gathering information for the design of hydraulic structures (Heller, 2011; Pfister & Chanson, 2012; Yalin, 1971). Among the studies on hydraulic jumps in physical models, notable ones include those conducted by Peterka (1984), Rajaratnam (1965a, 1965b, 1967), as well as the compiled and published data by Hager (1992) and Hager & Bremen (1989).

However, analyses based on hydraulic physical models also come with inherent errors, mainly due to the impossibility of achieving complete similarity (geometric, kinematic, and dynamic) between the model and the full-scale structure. The main differences found between prototype measurements and model measurements are caused by three primary types of effects: model effects, measurement effects, and scale effects (Heller, 2011).

In this context, computational modeling becomes an interesting approach for investigating complex phenomena, such as hydraulic jumps (Chanson, 2009b, 2009c; De Padova & Mossa, 2021). With the advent of modern computers with increased processing power and memory capacity, as well as the availability of cloud computing, it has become possible to computationally investigate more complex phenomena that require higher computational costs for their simulations. As a result, CFD simulations have become increasingly popular, even on personal computers.

Among the various techniques used, those based on Reynolds-Averaged Navier-Stokes (RANS) equations stand out, which are obtained by applying Reynolds decomposition to the Navier-Stokes equations. However, these equations have a closure problem, where it is necessary to model the term related to Reynolds stresses in the RANS equations. Numerous well-established references in fluid mechanics and turbulence study this topic (Bailly & Comte-Bellot, 2015; Lesieur, 2008; Pope, 2000; Wilcox, 2006).

RANS-based computational models have lower computational costs compared to, for example, Direct Numerical Simulation (DNS) models, which require extremely refined meshes to represent all turbulent scales in the simulated flow. Therefore, when conducting RANS-based simulations, it is assumed that not all turbulence scales are being simulated, and caution should be exercised when interpreting results related to these scales.

Validating results obtained in computational simulations often involves comparing them with other sources, such as measured data or well-established analytical or empirical equations. It is crucial to consider any inherent errors arising from the sources of the results, whether they originate from physical experiments (e.g., equipment precision and measurement errors) or computational simulations (e.g., numerical diffusion effects, inaccuracies in numerical models). Sharing such comparisons between simulations and data from physical experiments holds significant importance for advancing the science in the field.

Another significant challenge during the validation and calibration phase of computational simulations is the availability of measured data in the full-scale structures. The large dimensions observed in these structures, combined with the difficulty of instrumentation in highly turbulent, biphasic, and high-velocity flow, make intrusive measurements of these flows rare yet extremely valuable. In the Brazilian context, the pressure measurement campaign conducted at the bottom of the stilling basin of the Porto Colômbia Hydroelectric Power Plant stands out (Teixeira, 2008).

The present study aims to compare the results obtained from CFD simulations using RANS-based techniques with experimentally measured results from three hydraulic physical models at different scales (1:32, 1:50, and 1:100), as well as results measured at the full-scale structure. Additionally, this study aims to observe if there is any relationship between the simulated scale and the simulation results.

THEORETICAL BACKGROUND

The following section presents the theoretical framework that will serve as the basis for the comparisons in the results section. It is important to note that the hydraulic jump observed in the energy dissipation structure discussed here belongs to B-Jump category, as described by Kindsvater (1944, as cited in Hager, 1992).

The B-jump hydraulic jumps are characterized by their initiation in the sloped spillway channel and termination in the stilling basin. Therefore, all the results and comparisons presented below are derived from equations specific to this type of hydraulic jump. Figure 1 illustrates the characteristic variables of a B-jump hydraulic jump.

The Froude number, a widely used dimensionless parameter for characterizing free-surface flows, including hydraulic jumps, is defined by Equation 1 for the upstream section of the hydraulic jump:

$$Fr_1 = \frac{q\cos(\alpha)}{\sqrt{g\,h_1^3}} \tag{1}$$

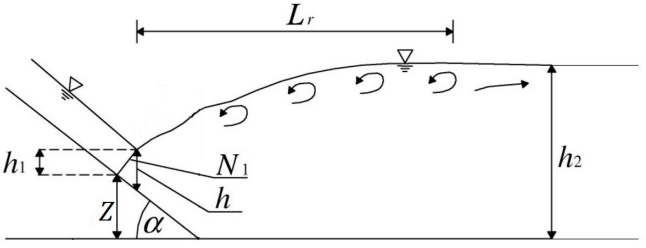

Figure 1. Typical B-jump characteristics. Adapted from Carollo et al. (2011).

where q represents the unit flow rate in $m^3/(s.m)$, α is the angle formed between the spillway channel and the stilling basin, g denotes the gravitational acceleration in m/s^2, and h_1 refers to the upstream conjugated depth of the hydraulic jump.

Prior to discussing the methodology employed in this study, a theoretical framework is presented regarding the analyzed variables. This framework provides a foundation for the comparisons presented in the results and discussions chapter of this work.

Mean pressure in stilling basin

Understanding the mean pressure at the bottom of hydraulic jump stilling basins, as well as pressure oscillations, extreme values, and their probability of occurrence, is of great importance for designing and sizing stilling basins in a safe and cost-effective manner.

Teixeira (2008) conducted an experimental investigation on mean pressures in the stilling basin of Porto Colômbia Hydroelectric Power Plant. The study involved measurements obtained from hydraulic physical models at different scales and measurements in the full-scale structure. The primary focus of Teixeira's (2008) work was to investigate the scale effect on the average pressures in this structure. However, the publication of the experimental pressure data alone holds great significance, especially for computational studies aiming to compare simulated and measured data, such as the study presented here.

Conjugated depths

The conjugate depths of a hydraulic jump have long been utilized as key variables in describing this phenomenon. Given the practical relevance of hydraulic jumps in engineering projects, new empirical equations have been developed and applied to various categories of hydraulic jumps to describe their conjugated depths.

Teixeira (2008), from whom a portion of the experimental data used in this study was obtained, employed water level measurements and applied them to one-dimensional equations of mass conservation, momentum, and energy. These calculations allowed for the determination of the downstream conjugated depth (h_2). Additionally, the Bélanger equation (Equation 2) was used to calculate the upstream conjugated depth (h_2^*).

$$\frac{h_2^*}{h_1} = \frac{1}{2}\left(-1+\sqrt{1+8Fr_1^2}\right) \tag{2}$$

Although the result obtained from Equation 2 does not directly represent the physically measurable quantity of the subcritical conjugated depth (h_2) in a B-jump hydraulic jump, it has been employed in the studies by Teixeira (2008), Teixeira et al. (2012), and Wiest et al. (2020) to calculate this variable and achieve dimensionless results. Therefore, to prevent any misinterpretation of the variables used in the equations of this study, the variable h_2^* will be maintained as the calculated subcritical conjugated depth derived from the Bélanger equation.

Other authors have also developed empirical equations specifically for calculating the subcritical conjugated depth in B-jumps (Carollo et al., 2011; Hager, 1988; Hager & Bremen, 1989; Kawagoshi & Hager, 1990).

Roller length

The roller length of a hydraulic jump is a critically important parameter as it represents the point where pressure fluctuations near the bottom become less pronounced, resulting in lower turbulent kinetic energy. This aspect holds significant relevance in the design of stilling basins, as it determines the optimal length required for effective dissipation. By accurately determining the roller length, unnecessary oversizing of the basin can be avoided, leading to substantial cost savings in the construction of the spillway facilities.

According to Hager et al. (1990), the roller length is defined as the point of velocity stagnation on the jump's free surface, marking the separation between downstream and upstream flow. Marques et al. (1997) identify the end of the roller as the region where the coefficient of pressure asymmetry reaches its minimum value. In physical experiments, determining this point can be challenging due to the complex and turbulent nature of the hydraulic jump. However, in computational simulations, visualizing the stagnation point becomes easier, facilitating the measurement of the hydraulic jump's roller length (Valero et al., 2018).

Two empirical equations have been found for calculating the roller length of B-jump (Adam et al., 1993; Carollo et al., 2012). Adam et al. (1993) derived an expression based on data from a physical experiment with channel slopes of 11.3°, 14.0°, and 18.4°, as presented in Equation 3.

$$\frac{L_r}{H_L} = 42.67\exp\left(-4.462\frac{H_L}{H_1}\right) \tag{3}$$

where L_r represents the roller length, H_L denotes the head loss in the hydraulic jump, given by $(H_1 - H_2)$, where H_1 and H_2 are the hydraulic head at the upstream and downstream sections of the jump, respectively.

Carollo et al. (2012) proposed a new empirical equation (Equation 4) for determining the roller length. This equation is applicable to both smooth and rough surface free hydraulic jumps, as well as smooth surface B-jump. The authors derived this equation based on experimental data obtained from channel angles ranging from 0° to 45°.

$$\frac{L_r}{H_L} = \left[7.965+20.72\left(\tan\alpha\right)^{0.39}\right]\left(\frac{H_L}{H_1}\right)^{-0.534} \exp\left(-\frac{H_L}{H_1}\frac{1}{0.168}\right) - \left[1-\exp\left(-\frac{H_L}{H_1}\frac{1}{0.168}\right)\right]4.124\ln\left(\frac{H_L}{H_1}\right) \tag{4}$$

where α represents the angle between the spillway and the stilling basin. The other variables are the same presented in Equation 3.

Water surface profile

The measurement of the water surface profile in hydraulic jumps, also known as the water level profile, can be challenging due

to the highly turbulent and two-phase nature of these phenomena. In hydraulic physical models, various instrumentation techniques have been employed to measure the water surface, such as the use of limnimetric probes and image capture methods (Teixeira, 2008). Non-intrusive measurement methods, including ultrasonic sensors (Nóbrega et al., 2014) and laser profilers (Macián-Pérez et al., 2020), have also been utilized for studying hydraulic jump characteristics.

In computational simulations, when employing methods based on scalar functions, such as the Volume of Fluid (VOF) method (Hirt & Nichols, 1981), the determination of the fluid fraction (α) representing the free surface of the flow becomes crucial. It is common to assume a phase equilibrium ($\alpha = 0.5$) to represent the free surface. However, capturing the water surface profile accurately, especially in the initial region of the jump where air entrainment occurs, remains a challenge due to the complex nature of hydraulic jumps (Chanson, 2009c; Marques et al., 2007).

Determining the precise location of the toe of a B-jump involves accurately calculating other variables that rely on this position during the design phase. The determination of the start position of the submerged jump also holds significance, for instance, in defining the elevations and dimensions of piers in weirs with controlled sills.

Wiest et al. (2020) developed an equation to determine the start height of B-jumps based on data measured in the 1:50 scale hydraulic model of the spillway and stilling basin of Porto Colômbia Hydropower Plant. In this study, the authors utilized measured data for flows ranging from 1,000 m³/s to 8,000 m³/s (full-scale), considering different degrees of submergence of the hydraulic jump. The authors presented the following equation (Equation 5) to define the variable z.

$$\frac{Z}{h_c} = \left[Fr_1 (S - 1) \right]^{0.61} \tag{5}$$

where z represents the difference in elevations between the start position of the hydraulic jump in the spillway channel and the bottom elevation of the stilling basin (see Figure 1), h_c denotes the critical flow depth for a rectangular channel, given by $h_c = \left(q^2 / g \right)^{1/3}$, and S represents the submergence of the jump, calculated as $S = T_W / h_2^*$, where T_W corresponds to the water depth in the downstream channel (tailwater).

Determining the correct horizontal position for toe of submerged hydraulic jumps also indirectly impacts the determination of other jump variables, such as the roller length. In physical modeling, establishing this position can be challenging due to the two-phase and turbulent characteristics of the flow, particularly in the initial regions of the hydraulic jump.

MATERIALS AND METHODS

The simulations were conducted to study the spillway and stilling basin of UHE Porto Colômbia. The weir of UHE Porto Colômbia is equipped with gate-controlled weir, and the stilling basin has approximately 163.0 meters in width and 45.8 meters in length. Originally, the stilling basin had a geometry resembling a USBR Type II basin. However, it underwent geometric alterations in response to structural issues caused by cavitation processes in the chute blocks and bottom slab. The changes made included the removal of the chute blocks at the basin's start and alterations to the geometry of the end-sill (Carvalho, 2010). Still, the observed hydraulic jump in this structure corresponds to a B-jump, as described by Kindsvater (1944, as cited in Hager, 1992).

Measured results from physical experiments, which will be compared with the simulation outcomes, were reported in works by Teixeira (2008), Wiest (2008), Teixeira et al. (2012), and Wiest et al. (2020). Additionally, other computational studies related to the spillway of UHE Porto Colômbia were examined (Amorim et al., 2004, 2015; Rodrigues, 2002).

The simulations were carried out using the Ansys CFX solver within the Ansys Workbench platform, which was also used for simulation domain modeling and mesh generation. A three-dimensional domain was employed, with sectional characteristics. Ansys CFX utilizes a finite volume approach for its numerical solutions, employing the RANS (Reynolds-Averaged Navier-Stokes) equations (Equations 6 and 7) for a Newtonian, incompressible fluid, presented below in tensorial format. A steady-state solution was adopted in Ansys CFX, using a pseudo-time-stepping approach until reaching the minimum residual or maximum iterations criteria.

$$\frac{\partial \overline{u_i}}{\partial x_i} = 0 \tag{6}$$

$$\rho \frac{\partial \overline{u_i}}{\partial t} + \rho \overline{u_j} \frac{\partial \overline{u_i}}{\partial x_j} = -\frac{\partial p}{\partial x_i} + \mu \frac{\partial^2 \overline{u_i}}{\partial x_j^2} - \rho \frac{\partial \overline{u_i' u_j'}}{\partial x_j} \tag{7}$$

The boundary conditions included a mass flow rate inlet condition at the upstream section, corresponding to a water flow rate of 4,000 m³/s (at full-scale); an outlet condition with a constant water level under hydrostatic pressure; no-slip wall conditions where no mass exchange occurs; symmetry conditions on the lateral domains; and open boundary conditions at the top domain. Figure 2 illustrates the boundary conditions, the simulation domain and the mesh adopted.

The air-water interface modeling was performed using the Volume of Fluid (VOF) method described by Hirt & Nichols (1981) in a homogeneous multiphase model, already implemented in the Ansys CFX solver (Ansys, 2009), widely used in computational modeling of hydraulic jumps (Bayon-Barrachina & Lopez-Jimenez, 2015; Bayon et al., 2016; Macián-Pérez et al., 2020; Valero et al., 2018). A water-air fraction $\alpha = 0.5$ was adopted to represent the balance between these phases and isosurfaces were traced from this value to aid in determining flow depths at various points and the position of the jump toe.

The hydraulic jump toe was determined as the location where the returning flow from the jump roller encounters the rapid flow over the weir channel with a water-air fraction $\alpha = 0.5$. From this point, the upstream conjugate depth (h_1) of the hydraulic jump was measured perpendicular to the weir chute, and the average velocity at this section was determined using a perpendicular plane to the weir, with the same width as the domain and depth h_1.

For the closure problem of the RANS equations and turbulence modeling, the RNG κ-ε model, proposed by Yakhot et al. (1992), was used. The RNG κ-ε model is a derivation of the traditional κ-ε model but with the advantage of being less dependent on empirical constants, making it more suitable for hydraulic jump simulations based on RANS (Amorim et al., 2015; Bayon-Barrachina

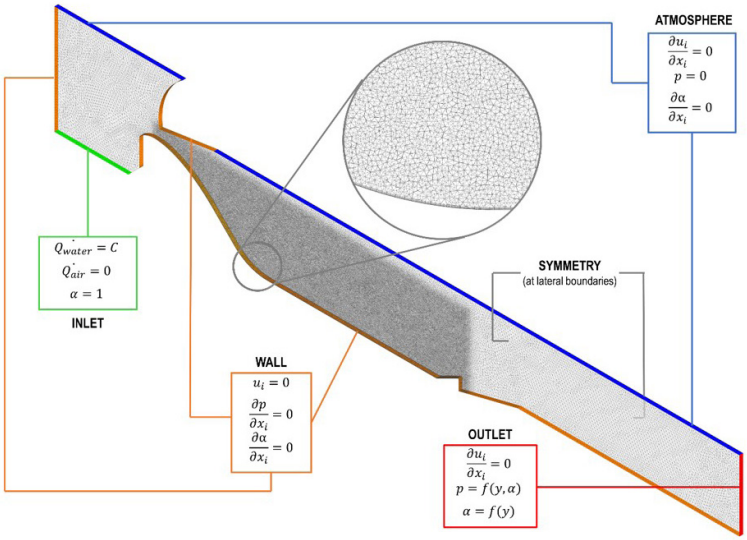

Figure 2. Simulation domain, boundary conditions and mesh.

& Lopez-Jimenez, 2015; Bayon et al., 2016; Macián-Pérez et al., 2020; Valero et al., 2018). The RNG κ-ε turbulence model is a two-equation model, where the first equation (Equation 8) represents the turbulent kinetic energy (κ), and the second one (Equation 9) determines the rate of turbulent kinetic energy dissipation (ε).

$$\frac{\partial(\rho k)}{\partial t}+\frac{\partial(\rho k u_i)}{\partial x_i}=\frac{\partial}{\partial x_j}\left[\left(\mu+\frac{\mu_t}{\sigma_k}\right)\frac{\partial k}{\partial x_j}\right]+G_k-G_B-\rho\varepsilon+S_k \tag{8}$$

$$\frac{\partial(\rho \varepsilon)}{\partial t}+\frac{\partial(\rho \varepsilon u_i)}{\partial x_i}=\frac{\partial}{\partial x_j}\left[\left(\mu+\frac{\mu_t}{\sigma_k}\right)\frac{\partial \varepsilon}{\partial x_j}\right]+ C_{1\varepsilon}\frac{\varepsilon}{k}\left(G_k+C_{3\varepsilon}G_B\right)-C_{2\varepsilon}\rho\frac{\varepsilon^2}{k}-R_\varepsilon+S_\varepsilon \tag{9}$$

where G_κ refers to the generation of turbulent kinetic energy caused by the mean velocity gradient; G_B refers to the generation of turbulent kinetic energy due to buoyancy, and; S_κ and S_ε are the source terms. The relationships for R_ε and μ_t, the latter being given in the effective viscosity term (μ_{eff}), are provided by Equations 10 and 11.

$$R_\varepsilon=\frac{C_\mu\rho\eta^3\left(1-\eta/\eta_0\right)\varepsilon^2}{k\left(1+\beta\eta^3\right)} \tag{10}$$

$$\mu=\frac{\rho C_\mu k^2}{\varepsilon} \tag{11}$$

where C_μ, $C_{1\varepsilon}$, $C_{2\varepsilon}$, $C_{3\varepsilon}$, σ_κ, σ_ε, η_0 and β are the RNG κ-ε model constants.

The mesh was generated using Ansys Meshing and consisted of a triangular pyramidal prismatic mesh with an inflation scheme starting from the weir channel wall, as can be seen in Figure 2. A mesh refinement was applied in the region of the hydraulic jump occurrence, within the stilling basin (see Figure 2). The elements in the refined region had characteristic dimensions of 0.16 m in full-scale, adjusted through geometric scaling for the desired simulation scale. The total number of mesh elements was about 3.010^6 elements.

Mesh definition and validation were carried out through the Grid Convergence Index (GCI) calculation. The GCI is an iterative method proposed by Roache (1997) and systematized by Celik et al. (2008) to assess numerical uncertainty by comparing variables obtained from simulations with different mesh discretizations. GCI was calculated based on average pressures at specific points of interest at the bottom of the channel for each of the four simulated scales. The coarse, medium, and fine mesh relationship in the region of the hydraulic jump occurrence was 40% ($l_{medium}/l_{coarse}=l_{fine}/l_{medium}=1.4$, where l represents the characteristic dimension of the mesh). The obtained average GCIs for the medium mesh were 3.66%, 2.78%, 3.21%, and 5.47% for scales 1:1, 1:32, 1:50, and 1:100, respectively, for the mean pressure analysis. Thus, by calculating the GCI using a coarse, medium, and fine mesh, the use of the medium mesh was validated, ensuring the independence of the simulation results with errors within the range of the calculated GCI's.

The simulation results were compared with measurements from physical hydraulic models at scales 1:32, 1:50, and 1:100, as well as full-scale data. Additionally, other variables that were not directly measured but were calculated indirectly were compared with empirical equations. The following variables were analyzed: mean pressures (P) at the bottom of the stilling basin; upstream hydraulic jump conjugated depth (h_1); roller length (L_R); water surface profile along the basin; submerged hydraulic jump inception depth (z) and velocity analysis along the hydraulic jump. Pressure and water level data, extracted from the works of Teixeira (2008) and Teixeira et al. (2012), were measured at specific locations along the channel and stilling basin, as presented in Figure 3. The measurement point nomenclature was preserved from Teixeira (2008) and Teixeira et al. (2012).

Pressure and water level measurement locations are shown in Figure 3. In the 1:32 scale model, the measurements were taken at all positions. In the 1:50 and 1:100 scale models, measurements

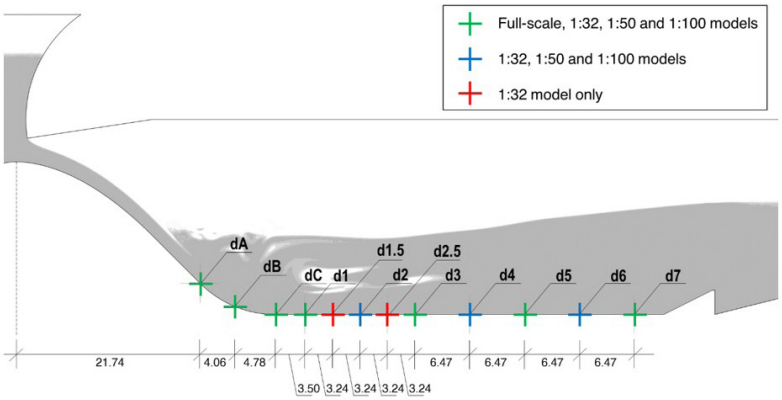

Figure 3. Pressure probe's locations. Measurements in full-scale.

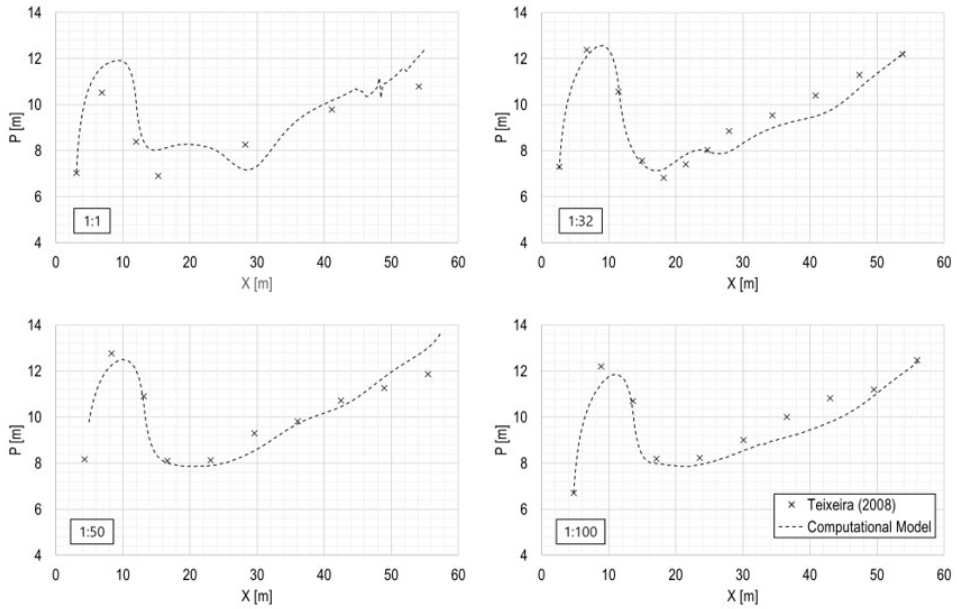

Figure 4. Mean pressures at bottom of the stilling basin. Values in full-scale.

were not taken at the d1.5 and d2.5 probe locations, while in the full-scale structure, measurements were not taken at the d1.5, d2, d2.5, d4, and d6 probe locations. For more detailed information on the instrumentation of the models and the prototype, refer to Teixeira (2008), Wiest (2008), Carvalho (2010), Teixeira et al. (2012), and Wiest et al. (2020).

RESULTS AND DISCUSSION

The study results will be presented and discussed in the same order as addressed in the theoretical framework: mean pressures at the bottom of the stilling basin, upstream conjugated depth, jump roller length, waterline profile, and velocity analysis.

Figure 4 shows the simulation results for the mean pressures at the bottom of the stilling basin for the four different simulated scales, compared with the average pressure results presented by Teixeira (2008) for the same structure. The x-axis origins are relative to the onset of the hydraulic jump, and the pressure data, presented in meters of water column, have been scaled to full-scale.

The mean pressure data obtained in the simulations satisfactorily reflect the trend observed in the values measured in the three small-scale physical models. However, in the full-scale (prototype), there is a greater variation between the simulated and observed data, with overestimation of the average pressures at the concordance curve and the beginning of the energy dissipation basin. Additionally, a decrease in the average pressure at $x \cong 12$ is observed. Table 1 presents the observed relative pressure errors and their average for each simulated scale.

From the analysis of the errors presented in Table 1, it is also observed that 50% of these errors are smaller than the mesh-related uncertainty, calculated by GCI, for average pressures at the 1:32 scale, 60% for the 1:50 scale, and 40% for the 1:100 scale. However, for the mean pressure results at the full-scale, all observed errors were larger than the mesh-related uncertainty.

Another notable observation is regarding the peak pressure observed at the concordance curve. Due to the change in flow direction at the concordance curve, centrifugal inertial forces manifest due to the presence of vertical and normal accelerations

Table 1. Comparison of mean pressures between observed data (Teixeira, 2008) and simulated results.

Probe	Mean Pressure (m)								Difference (%)			
	Teixeira (2008)				Simulation							
	1:1	1:32	1:50	1:100	1:1	1:32	1:50	1:100	1:1	1:32	1:50	1:100
dA	7.03	7.30	8.16	6.71	7.11	7.38	7.94	7.21	1.1	1.1	2.7	7.5
dB	10.52	12.37	12.77	12.21	11.62	12.13	12.26	11.55	10.5	2.0	4.0	5.4
dC	8.39	10.57	10.90	10.69	10.17	10.71	10.57	10.07	21.2	1.3	3.0	5.8
d1	6.91	7.57	8.10	8.20	8.04	7.42	8.03	7.55	16.4	1.9	0.9	7.9
d1.5	-	6.83	-	-	-	7.22			-	5.6	-	-
d2	-	7.40	8.13	8.24	-	7.83	7.91	8.09	-	5.8	2.7	1.9
d2.5	-	8.03	-	-	-	7.98			-	0.7	-	-
d3	8.27	8.86	9.29	9.01	7.18	7.97	8.53	8.43	13.2	10.1	8.2	6.4
d4	-	9.54	9.83	10.00	-	9.00	9.71	8.91	-	5.7	1.2	10.9
d5	9.79	10.40	10.73	10.83	10.18	9.51	10.46	9.52	3.9	8.5	2.5	12.1
d6	-	11.29	11.25	11.19	-	10.73	11.75	11.10	-	5.0	4.4	0.8
d7	10.80	12.19	11.88	12.47	12.09	12.25	13.03	12.47	11.9	0.5	9.7	0.0

Values in full-scale.

to the flow. The effect of this force gradually increases toward the center of the curve, where the maximum average pressure is observed (Linfu & Jie, 1985, as cited in Prá et al., 2012). However, in Figure 4, it can be seen that the point of maximum average pressure is located beyond the central point of the curve, at $X \cong 8$.

For the determination of water levels obtained in the simulations, a water-air interface fraction $\alpha = 0.5$ was considered as the interface between these fluids. The values of the upstream conjugated depth (h_1) obtained in the simulations were compared with the results calculated by Teixeira (2008). Table 2 presents this comparison and the average difference between these values.

The simulation results closely match the values calculated by Teixeira (2008) for this variable, with relative percentage differences ranging from 1.19% to 6.57%. It is a common practice among engineers that designs stilling basin structures to calculate the upstream conjugated depth of a hydraulic jump using one-dimensional mass and energy conservation equations, as done by Teixeira (2008). Therefore, the CFD simulations, for the given conditions and models, prove to be satisfactory in calculating this variable.

The statement by Valero et al. (2018) that the region of the hydraulic jump roller can be easily defined in computational simulations is supported by the results depicted in Figure 5. The magnitudes of velocities in the longitudinal direction were filtered between positive and negative values, revealing the stagnation point.

Thus, the positions marking the end of the hydraulic jump roller were easily defined for all scales, enabling the measurement of the roller length. The simulation results were then compared with two empirical equations presented in the theoretical framework, as shown in Table 3.

The hydraulic jump roller lengths calculated using Equation 4 (Carollo et al., 2012) showed the smallest average variation among the scales compared to the simulated data, with a mean difference of 6.1%.

Another dataset provided by Teixeira (2008) includes flow depths along the hydraulic jump, measured at the same location as the previously presented pressure measurements. The data were collected for the three tested model scales (1:32, 1:50, and 1:100), and the comparison between the simulated and observed data is depicted in Figure 6.

Table 2. Comparison of h_1 values calculated by Teixeira (2008) and simulation results.

Scale	h_1 [m]		Difference (%)
	Teixeira (2008)	Simulation	
1:1	1.179	1.120	4.93
1:32	1.161	1.085	6.57
1:50	1.197	1.154	3.52
1:100	1.181	1.167	1.19

It can be observed that the water surface profile is overestimated in the simulations at positions near the first four locations (dA, dB, dC, and d1), in $0 < X \leq 16$, which are located at the convergence curve and the beginning of the stilling basin. The error for these positions across all scales averages 43.4%. However, the simulated water levels at the final probe locations (d3, d5, and d7), in $X > 16$, show good agreement with the observed data published by Teixeira (2008), with an average error of 4.0%. The main hypothesis that the largest differences are found in the region near the jump toe arises from the difficulty of computationally represent the aeration phenomenon of the hydraulic jump. As showed in the materials and methods of this work, the VOF method was used to model the interaction between phases water and air, which may not have proven to be the most suitable for modeling the zone with highest air concentrations of the simulated phenomenon.

As described by Teixeira (2008), water level measurements in the physical experiments were taken using limnimeter tips. According to Marques et al. (1997), the regions with the highest pressure fluctuations are located near point $1.75(h_2 - h_1)$. Furthermore, according to Marques et al. (2007), the aeration region extends from the beginning of the hydraulic jump to the point of maximum air concentration, which corresponds to the region of maximum pressure fluctuations. Consequently, obtaining water level measurements in this zone using limnimeter tips poses challenges and tends to also yield higher errors.

Table 3. Comparison of simulated and empirically calculated lengths of the hydraulic jump roller.

Scale	L_R [m]			$\lvert L_{R,Sim.} - L_{R,Calc.} \rvert / L_{R,Sim.}$ [%]	
	Sim.	Equation 3	Equation 4	Equation 3	Equation 4
1:1	64.8	55.1	58.1	14.9	10.3
1:32	62.9	55.4	58.3	11.9	7.2
1:50	63.8	58.2	61.4	8.8	3.8
1:100	61.7	56.5	59.9	8.5	3.0

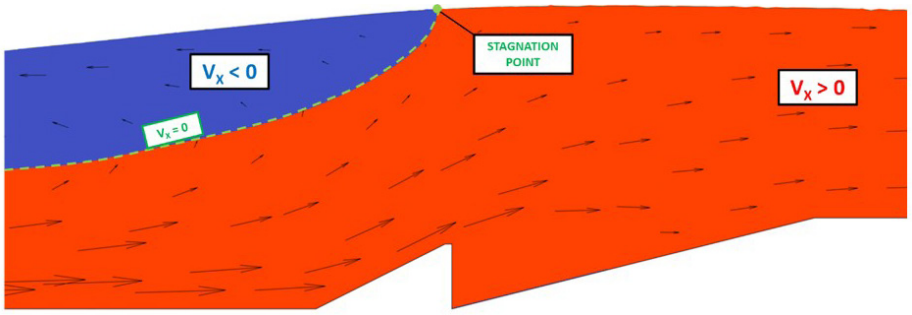

Figure 5. Stagnation point visualization, marking the end of the hydraulic jump roller.

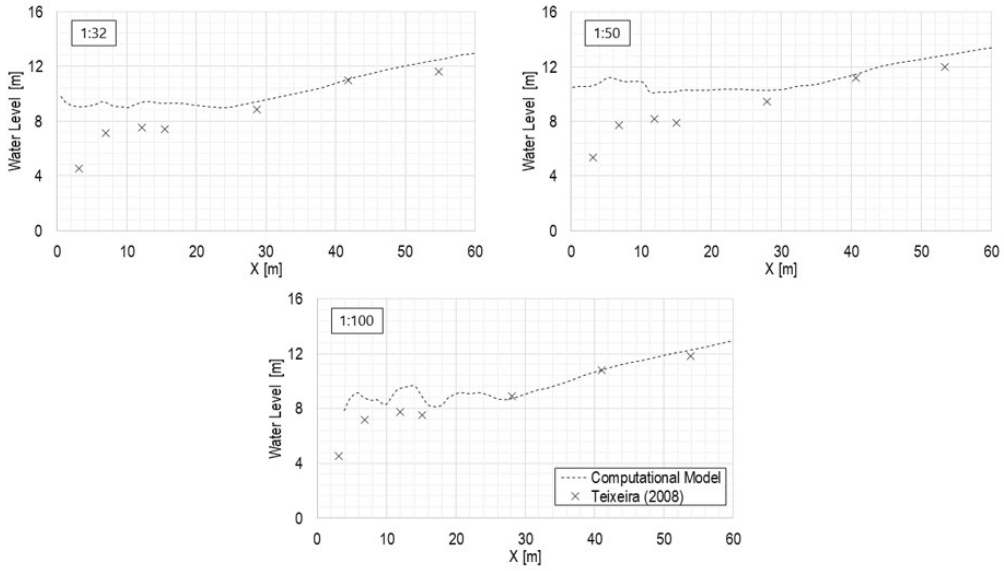

Figure 6. Comparison between simulated and observed (Teixeira, 2008) water surface profiles.

The start height of the submerged hydraulic jump was compared between the simulation results and the equation proposed by Wiest et al. (2020), shown in Equation 5. The comparison is illustrated in Figure 7.

Regarding the calculation of submergence ($S = T_W / h_2^*$) from the simulated data, h_2^* values were utilized, computed based on the Bélanger equation (Equation 5). This approach was adopted since Wiest et al. (2020) also derived their Equation 5 using h_2^* data.

The CFD simulations, under the given conditions and models, exhibited variations of 11.7%, 19.5%, and 11.8% when compared to Equation 5 for scales 1:1, 1:32, and 1:50, respectively. However, the results obtained in the 1:100 scale simulation for this variable were underestimated by 59.3% compared to Equation 5, indicating a start depth lower than the one calculated by Wiest et al. (2020).

The 1:100 scale simulation, unlike the other scales, showed higher uncertainty regarding the observed water-air fractions in the jump toe region, making it challenging to locate the start of the hydraulic jump. Figure 8 illustrates this difficulty, where the toe of the submerged hydraulic jump in the 1:100 scale simulation does not exhibit the same contour uniformity as the results for the other scales.

However, it is important to consider that the start positions of the hydraulic jump reported by Wiest et al. (2020) were measured using limnimeter tips, and as described in the theoretical framework, these measurements are challenging due to the high air concentration and turbulence in this region.

The present study employed the VOF method to resolve multiphase flow and solve the transport equations at the water-air interface. It should be noted that this method may not accurately represent aeration phenomena at scales smaller than the simulation mesh (Torres et al., 2021). While the method was not specifically designed for hydraulic jumps but for stepped spillways, van Alwon (2019) suggested that VOF may not be suitable for analyzing air entrainment in the flow. Moreover, Lopes et al. (2018), also studying a stepped spillway, pointed out that the VOF model lacks a global value of the water-air fraction to accurately represent the free surface. Thus, a dedicated study is necessary to evaluate the aeration phenomenon in the structure under analysis.

Although the previous works reporting results from measurements in hydraulic physical models and the prototype (Teixeira, 2008; Teixeira et al., 2012; Wiest, 2008; Wiest et al., 2020) of the simulated structure did not provide velocity data, the simulation results for the same will be presented and discussed. Figure 9 displays the absolute velocity fields for the four simulated scales.

The flow velocity magnitudes and recirculation patterns remain consistent across different scales. Teixeira (2008) employed one-dimensional mass and energy conservation equations to compute the velocity at the upstream section of the hydraulic jump (V_1), which was then used to determine the flow depth at the same location, using the same equations. Table 4 presents a comparison between the velocities calculated by Teixeira (2008) and the average velocities obtained in the simulation for the upstream section of the hydraulic jump, derived from the average velocity vectors in a plane perpendicular to the flow.

Both methodologies yield similar results, with variations ranging from 2.6% to 5.3% across different scales. However, it is essential to note that both results lack a direct comparison with measured velocity data at the starting position of the hydraulic jump, which would enable a more reliable assessment of the calculated and simulated results against the actual measurements.

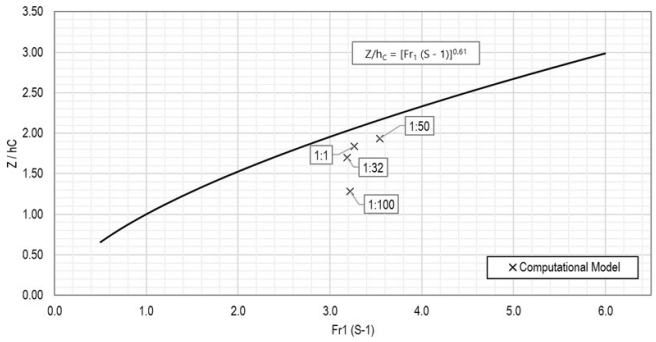

Figure 7. Comparison between the equation proposed by Wiest et al. (2020) and simulation results.

Table 4. Comparison of upstream velocities of the hydraulic jump calculated by Teixeira (2008) and obtained in the simulation.

Scale	V_1 [m/s]		Difference (%)
	Teixeira (2008)	Simulation	
1:1	17.69	18.39	3.95
1:32	17.51	18.05	3.03
1:50	18.04	17.08	5.31
1:100	17.78	17.31	2.63

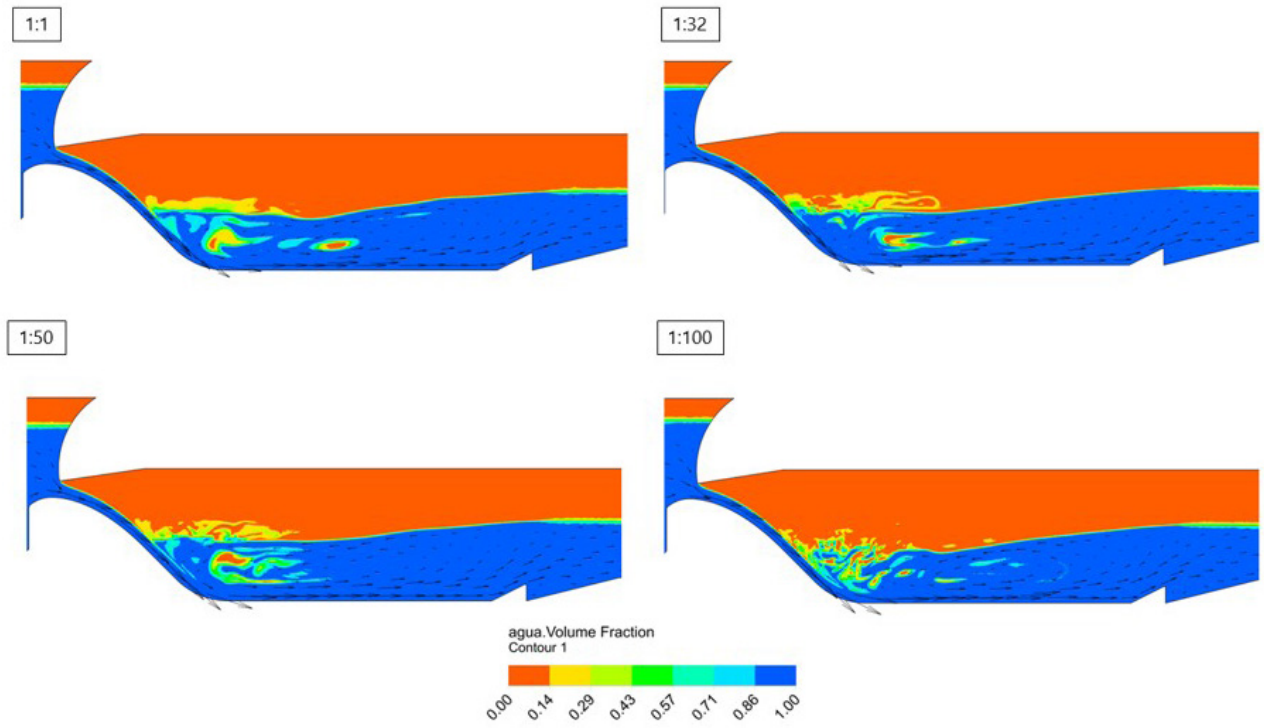

Figure 8. Air-water fraction results.

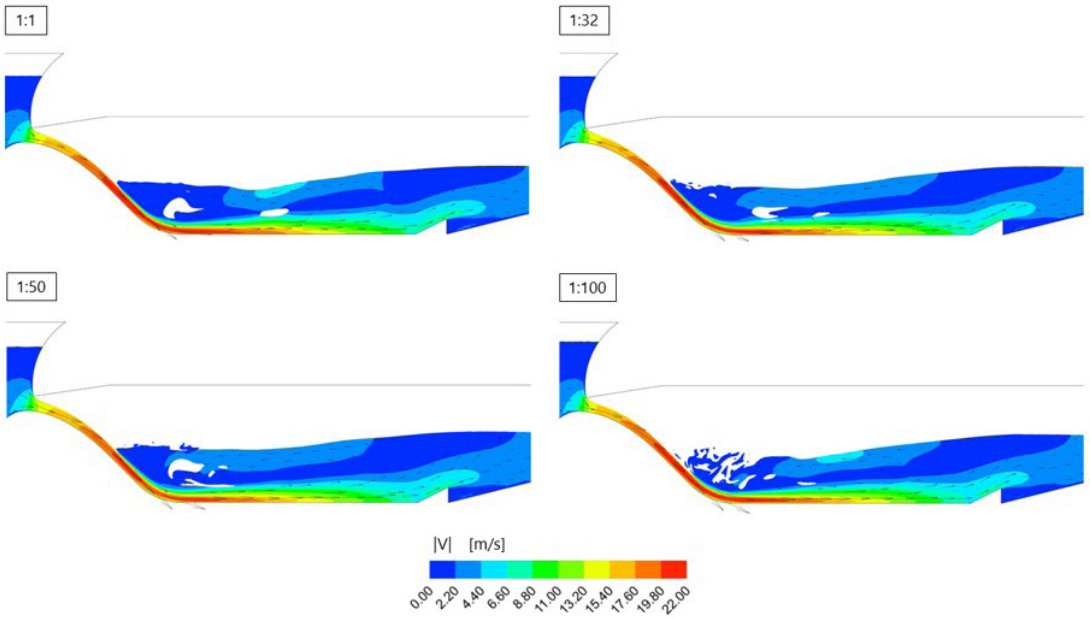

Figure 9. Velocity contours for all scales. Values in full-scale.

CONCLUSIONS

The present study conducted a comparison between CFD simulation results, well-established empirical equations, and measurements obtained from hydraulic physical models at three scales (1:32, 1:50, and 1:100) as well as the full-scale (1:1). The simulation methodology employed the Ansys CFX software, utilizing the RANS equations for steady-state solution and the RNG κ-ε turbulence model for turbulence modeling, along with the VOF method for water-air interface representation.

The obtained simulation results were compared with experimentally measured variables (mean pressures at the bottom of the stilling basin and waterline profiles), as well as indirectly calculated or empirically derived variables (conjugate depths, start position of the hydraulic jump, roller length, and velocity analysis).

Overall, the findings demonstrate that CFD simulations are a valuable tool for determining the magnitudes of the analyzed variables and can be effectively utilized for engineering design purposes in hydraulic jump stilling basins. Notably, computational simulations allow for the extraction of variable results at any desired point within the simulation domain through direct extraction or interpolation.

It is important to note that the simulation results in the proximity of the jump toe, where representing aeration in the flow using the VOF method posed challenges, exhibited greater discrepancies when compared to experimentally measured values or results derived from empirical equations. However, it is crucial to acknowledge that obtaining measurements in this turbulent and highly aerated flow region is also challenging in hydraulic physical models. In addition to uncertainties associated with the complex two-phase nature of flows in the initial jump region, this area is characterized by highly turbulent and intricate flow dynamics.

There were no significant differences observed among the simulated scales, except for the start position of the submerged jump in the 1:100 scale simulation. Nevertheless, it is worth noting that mean pressures at the bottom of the stilling basin were higher in the 1:32 and 1:50 scale simulations compared to the 1:1 scale, indicating the presence of scale effects also in the computational modeling, in addition to the scale effects previously reported by Teixeira (2008) in hydraulic physical models.

Considering that the computational simulations satisfactorily represent the analyzed variables across the four different simulated scales, it is noted that CFD simulations can also help in the analysis of scale effects in hydraulic structures. In this way, CFD simulations can complement the scale effect analysis already conducted through physical hydraulic models, allowing for greater variability of experimental conditions and the measurement of parameters that are impossible to capture through physical model instrumentation.

For future studies, it is recommended to conduct simulations under various computational conditions, including different turbulence models and approaches for multiphase water-air interface modeling. Additionally, comparing the presented solutions with results obtained from other software and solvers, such as the open-source package OpenFOAM, would be beneficial. To further enhance the analysis, conducting simulations for different flow rates and conditions, as well as submergence scenarios outlined by Teixeira (2008), and comparing these results with experimental data, will provide a more comprehensive understanding. Increasing the range of simulated flow rates will strengthen the data presented and solidify the comparisons made.

ACKNOWLEDGEMENTS

The authors would like to thank CNPq for the master's scholarship awarded to the first author during the development of this work, to Furnas Centrais Elétricas S. A. and Instituto de Pesquisas Hidráulicas for their support.

REFERENCES

Adam, A. M., Ruff, J. F., AlQaser, G., & Abt, S. R. (1993). Characteristics of B-jump with different toe locations. *Journal of Hydraulic Engineering*, *119*(8), 938-948.

Amorim, J. C. C., Rodrigues, R. C., & Marques, M. G. (2004). A numerical and experimental study of hydraulic jump stilling basin. *Advances in Hydroscience and Engineering*, *6*, 1-10.

Amorim, J. C. C., Rodrigues, R. C., & Barbosa, V. H. (2015). Experimental and numerical modeling of flow in a stilling basin. In *Proceedings of the 36th IAHR World Congress* (pp. 1-6), Hague, Netherlands.

Ansys. (2009). *ANSYS CFX: solver theory guide*. Canonsburg, PA: Ansys Inc.

Bailly, C., & Comte-Bellot, G. (2015). *Turbulence*. Cham: Springer International Publishing.

Bayon, A., Valero, D., García-Bartual, R., Vallés-Morán, F. J., & López-Jiménez, P. A. (2016). Performance assessment of OpenFOAM and FLOW-3D in the numerical modeling of a low Reynolds number hydraulic jump. *Environmental Modelling & Software*, *80*, 322-335. http://dx.doi.org/10.1016/j.envsoft.2016.02.018.

Bayon-Barrachina, A., & Lopez-Jimenez, P. A. (2015). Numerical analysis of hydraulic jumps using OpenFOAM. *Journal of Hydroinformatics*, *17*(4), 662-678. http://dx.doi.org/10.2166/hydro.2015.041.

Carollo, F. G., Ferro, V., & Pampalone, V. (2011). Sequent depth ratio of a B-jump. *Journal of Hydraulic Engineering*, *137*(6), 651-658.

Carollo, F. G., Ferro, V., & Pampalone, V. (2012). New expression of the hydraulic jump roller length. *Journal of Hydraulic Engineering*, *138*(11), 995-999.

Carvalho, E. (2010). O vertedouro de Porto Colômbia: desempenho e recuperação da bacia de dissipação. In: Comitê Brasileiro de Barragens, editor. *Grandes vertedouros brasileiros* (pp. 129-138). Rio de Janeiro: CBDB.

Celik, I. B., Ghia, U., Roache, P. J., Freitas, C. J., Coleman, H., & Raad, P. E. (2008). Procedure for estimation and reporting of uncertainty due to discretization in CFD applications. *Journal of Fluids Engineering, Transactions of the ASME*, *130*(7), 0780011-0780014.

Chanson, H. (2009a). Current knowledge in hydraulic jumps and related phenomena: a survey of experimental results. *European Journal of Mechanics - B/Fluids*, *28*(2), 191-210.

Chanson, H. (2009b). Development of the Bélanger Equation and Backwater Equation by Jean-Baptiste Bélanger (1828). *Journal of Hydraulic Engineering*, *135*(3), 159-163.

Chanson, H. (2009c). Turbulent air-water flows in hydraulic structures: dynamic similarity and scale effects. *Environmental Fluid Mechanics*, *9*(2), 125-142.

De Padova, D., & Mossa, M. (2021). Hydraulic jump: a brief history and research challenges. *Water*, *13*(13), 1733.

Hager, W. H. (1988). B-jump in sloping channel. *Journal of Hydraulic Research*, *26*(5), 539-558.

Hager, W. H. (1992). *Energy dissipators and hydraulic jump* (Vol. 8). Dordrecht: Springer Netherlands.

Hager, W. H., & Bremen, R. (1989). Classical hydraulic jump: sequent depths. *Journal of Hydraulic Research*, *27*(5), 565-585.

Hager, W. H., Bremen, R., & Kawagoshi, N. (1990). Classical hydraulic jump: length of roller. *Journal of Hydraulic Research*, *28*(5), 591-608.

Heller, V. (2011). Scale effects in physical hydraulic engineering models. *Journal of Hydraulic Research*, *49*(3), 293-306.

Hirt, C. W., & Nichols, B. (1981). Volume of Fluid (VOF) method for the dynamics of free boundaries. *Journal of Computational Physics*, *39*(1), 201-225.

Kawagoshi, N., & Hager, W. H. (1990). B-jump in sloping channel, II. *Journal of Hydraulic Research*, *28*(4), 461-480.

Lesieur, M. (2008). *Turbulence in fluids*. Dordrecht: Springer.

Lopes, P., Leandro, J., & Carvalho, R. F. (2018). Numerical procedure for free-surface detection using a volume-of-fluid model. *Journal of Hydro-environment Research*, *21*, 43-51.

Macián-Pérez, J. F., Vallés-Morán, F. J., Sánchez-Gómez, S., De-Rossi-Estrada, M., & García-Bartual, R. (2020). Experimental characterization of the hydraulic jump profile and velocity distribution in a stilling basin physical model. *Water*, *12*(6), 1758.

Marques, M. G., Drapeau, J., & Verrette, J.-L. (1997). Flutuação de pressão em um ressalto hidráulico. *Revista Brasileira de Recursos Hídricos*, *2*(2), 45-52.

Marques, M. G., Prá, M. D., Augusto, A., & Alves, M. (2007). Paralelo entre o coeficiente de aeração e a flutuação de pressão no ressalto hidráulico: um estudo teórico-experimental. In *Anais do XVII Simpósio Brasileiro de Recursos Hídricos*, São Paulo.

Nóbrega, J. D., Schulz, H. E., & Zhu, D. Z. (2014). Free surface detection in hydraulic jumps through image analysis and ultrasonic sensor measurements. In *Proceedings of the 5th IAHR International Symposium on Hydraulic Structures. Hydraulic Structures and Society - Engineering Challenges and Extremes*. Brisbane, Australia: The University of Queensland.

Peterka, A. J. (1984). *Hydraulic design of stilling basins and energy dissipators*. Denver, CO: United States Department of the Interior Bureau of Reclamation.

Pfister, M., & Chanson, H. (2012). Scale effects in physical hydraulic engineering models. *Journal of Hydraulic Research*, *50*(2), 244-246.

Pope, S. B. (2000). *Turbulent flows*. Cambridge: Cambridge University Press.

Prá, M. D. (2011). *Uma abordagem para determinação das pressões junto ao fundo de dissipadores de energia por ressalto hidráulico* (Tese de doutorado). Universidade Federal do Rio Grande do Sul, Porto Alegre.

Prá, M. D., Collares, G., Alves, A., & Marques, M. (2012). Pressões médias e flutuantes devidas ao escoamento em uma curva de concordância vertical entre vertedouro e canal horizontal: estudo experimental. *Revista Brasileira de Recursos Hídricos*, *17*(3), 197-207.

Rajaratnam, N. (1965a). Submerged hydraulic jump. *Journal of the Hydraulics Division*, *91*(4), 71-96.

Rajaratnam, N. (1965b). The hydraulic jump as a well jet. *Journal of the Hydraulics Division*, *91*(5), 107-132.

Rajaratnam, N. (1967). Hydraulic jumps. In: Chow VT, editor. *Advances in hydroscience* (Vol. 4, pp. 197-280). Orlando: Academic Press.

Roache, P. (1997). Quantification of uncertainty in computational fluid dynamics. *Annual Review of Fluid Mechanics*, *29*(1), 123-160.

Rodrigues, R. C. (2002). *Estudo numérico e experimental de bacia de dissipação* (Dissertação de mestrado). Instituto Militar de Engenharia, Rio de Janeiro.

Teixeira, E. D. (2008). *Efeito de escala na previsão dos valores extremos de pressão junto ao fundo em bacias de dissipação por ressalto hidráulico* (Tese de doutorado). Universidade Federal do Rio Grande do Sul, Porto Alegre.

Teixeira, E. D., Prá, M. D., Wiest, R. A., & Marques, M. G. (2012). Efeito de escala nos valores de pressão média junto ao fundo em bacias de dissipação por ressalto hidráulico submergido. *Revista Brasileira de Recursos Hídricos*, *17*(2), 87-100.

Torres, C., Borman, D., Sleigh, A., & Neeve, D. (2021). Application of three-dimensional CFD VOF to characterize free-surface flow over trapezoidal labyrinth weir and spillway. *Journal of Hydraulic Engineering*, *147*(3), 1-19.

Valero, D., Bung, D. B., & Crookston, B. M. (2018). Energy dissipation of a type III basin under design and adverse conditions for stepped and smooth spillways. *Journal of Hydraulic Engineering*, *144*(7), 04018036.

van Alwon, J. C. (2019). *Numerical modelling of aerated flows over stepped spillways*. Leeds, UK: University of Leeds.

Wiest, R. A. (2008). *Avaliação do campo de pressões em ressalto hidráulico formado a jusante de um vertedouro com diferentes graus de submergência* (Dissertação de mestrado). Universidade Federal do Rio Grande do Sul, Porto Alegre.

Wiest, R. A., Steinke Júnior, R., Teixeira, E. D., Prá, M. D., Aloysio, P. M. S., & Marques, M. G. (2020). Start position of a sloping hydraulic jump. *Revista Brasileira de Recursos Hídricos*, *25*, e19.

Wilcox, D. C. (2006). *Turbulence modeling for CFD* (3rd ed.). La Cañada, CA: DCW Industries.

Yakhot, V., Orszag, S. A., Thangam, S., Gatski, T. B., & Speziale, C. G. (1992). Development of turbulence models for shear flows by a double expansion technique. *Physics of Fluids. A, Fluid Dynamics*, *4*(7), 1510-1520.

Yalin, M. S. (1971). *Theory of hydraulic models*. London: Macmillan Education.

Authors contributions

João Pedro Paludo Bocchi: Conducted the computational runs, data extraction and analysis, text writing and image rendering.

Daniela Guzzon Sanagiotto: Technical and text review, provision of data from hydraulic physical models.

Eder Daniel Teixeira: Technical and text review, provision of data from hydraulic physical models.